Desalination and Water Treatment
www.deswater.com
doi: 10.5004/dwt.2023.29565

(2023) 1–12

Adsorption of Direct red 81 dye onto friendly prepared iron oxide/multi-walled carbon nanotubes nanocomposite: kinetics and thermodynamic studies

Haifa S. Elbogami[a], Rehab G. El-Sharkawy[b], Basma A.A. Balboul[a,*]

[a]*Chemistry Department, College of Science, Jouf University, P.O. Box: 2014, Sakaka, Aljouf, Saudi Arabia, emails: babalboul@ju.edu.sa (B.A.A. Balboul), haifaalrajhi11@gmail.com (H.S. Elbogami)*
[b]*Chemistry Department, Faculty of Science, Tanta University, Tanta, Egypt, email: relsharkawy78@gmail.com*

Received 31 December 2022; Accepted 18 April 2023

ABSTRACT

This paper describes the synthesis of an iron oxide/multi-walled carbon nanotubes (Fe_2O_3/MWCNT) nanocomposite for the removal of Direct red 81 dye as an organic pollutant. The nanocomposite was characterized using various techniques, including X-ray diffraction, Fourier-transform infrared spectroscopy, thermogravimetric analysis, UV-visible spectrophotometry, scanning electron microscopy, and transmission electron microscopy. The study demonstrates the feasibility of preparing a nanocomposite through a simple impregnation followed by a decomposition solid-state reaction, which reduces time and chemical costs. The characteristics of the nanocomposite and the kinetics of the adsorptive removal of the organic dye are described in detail, including the factors that govern adsorptive behavior such as pH, temperature, initial concentration of the dye, and adsorbent dosage. The results show that the efficiency of the adsorption process increases with increasing concentration of reactants and temperature. The study used Langmuir and Freundlich adsorption isothermal models, and the equilibrium data revealed that the Langmuir model fit linearly with the Direct red 81 adsorption, with the highest adsorption capacity being 73.05 mg/g. Additionally, the kinetics of the process fit linearly with the pseudo-second-order model. The thermodynamic studies showed that the adsorption process was endothermic and spontaneous, with a negative value of free energy change indicating favorable adsorption. Finally, a reusability study showed that the prepared composite had good decolorization performance over four consecutive cycles, indicating its potential as an effective and efficient adsorbent for the removal of organic pollutants.

Keywords: Multi-walled carbon nanotubes (MWCNTs) nanocomposite; Friendly preparation; Ammonium ferric citrate; Direct red 81 dye; Adsorption isotherms; Kinetics

1. Introduction

The toxic nature of organic dyes makes them a major contaminant in industrial wastewater and a potential cause of various health problems in humans. Worldwide, thousands of tons of dyes are produced annually, with nearly 60% being azo dyes. Direct red 81, a sulfonated azo-based dye, is both toxic and carcinogenic. Consuming large amounts of this dye can result in gastrointestinal disease, and may cause nausea, vomiting, and harmful effects on the skin and eyes. Despite its toxicity, Direct red 81 is widely used in many industries [1] due to its water solubility, which is facilitated by the presence of a double azo linkage and a sulfonic acid group [2].

There are several methods for treating water pollutants, including physical, chemical, and biological approaches [3]. One of the most effective and low-cost methods is adsorption, which relies on efficient adsorbents. A variety of materials have been used as adsorbents to eliminate contaminants from industrial water, including carbon-based materials like activated carbon (AC), carbon nanotubes, graphene oxide, aerogel carbon, polymeric matter, and waste-derived materials [3]. The field of adsorbent materials is rapidly growing, with carbon-based materials showing promise due to their

* Corresponding author.

Presented at the International Conference on New Trends in Renewable Energy and Environment for 2030 Vision (ICNTREE 2022), 24–26 January 2023, Jouf, Saudi Arabia

designed structures, morphologies, and functional groups. Multi-walled carbon nanotubes (MWCNTs) and graphene oxide are among the materials that have been successfully used to remove pollutants, thanks to their unusual chemical and physical properties. Surface area, surface functional groups, and the presence of conventional adsorbents like chitosan, polymers, zeolites, and Fe_3O_4 are key factors that govern the adsorption and catalytic performance of carbon nanotubes (CNTs) and graphene oxide-based materials [4,5]. By functionalizing the adsorbent surface and loading metals and/or metal oxides with controlled proportions, the efficiency of these materials can be increased in adsorption and degradation processes [5–7].

Ammonium ferric citrate, the green form of which is considered the source of iron oxide in this study, is an important material used for various applications. It has biological activity and medical uses, and has been used as a nutritional supplement for the treatment of iron deficiency anaemia. It can also be used as a food preservative, as it has a relatively high copper content. Additionally, it is widely used in industrial production and as a precursor for fabricating iron-oxide films and preparing Fe_2O_3 nanoparticles [8–11]. Fe_2O_3, the final thermal decomposition product of ferric oxide, has many applications in industrial fields such as catalysis and the formation of ferrite spinel's that possess distinctive electric and magnetic properties important in the electronic industry [12]. To our knowledge, the formation course of ferric oxide from the green form has not been previously reported in the literature. Various approaches for decorating ferric oxide onto CNTs have been reported, including high-temperature decomposition, precipitation, solvothermal, hydrothermal, and sol–gel methods [5–7,13–16].

In this study, Direct red 81 dye (DR81) was chosen as a model to investigate the adsorption activity of a nanocomposite made from ferric oxide and carbon nanotubes, which is abbreviated as iron oxide/carbon nanotubes (Fe_2O_3/CNT). The nanocomposite is prepared using a simple, environmentally friendly approach. To our knowledge, the formation course of ferric oxide from the green form has not been previously reported in the literature. The techniques used are X-ray diffraction, Fourier-transform infrared spectroscopy (FTIR), scanning electron microscopy (SEM), and thermogravimetric analysis (TGA) to describe the prepared materials, and evaluated the adsorption isotherms of DR81 onto Fe_2O_3/multi-walled carbon nanotubes (Fe_2O_3/MWCNT) under different conditions, such as pH, amount of adsorbent, initial DR81 concentration, and contact time. Additionally, the adsorption kinetics, isotherm, and thermodynamics were investigated. The goal of this study is to utilize reactive nanocomposite of carbon nanotubes modified by hematite nanoparticles, which is prepared using a low-cost, environmentally friendly approach, for the treatment of organic pollutants. Specifically, the aim was to identify the variables that affect the nanocomposite's reactivity, decolorization kinetics, and mechanism.

2. Experimental set-up

2.1. Chemicals and characterization methods

The ammonium ferric citrate hydrate, abbreviated as AFC, used in this study is green colored and has a linear formula of $C_6H_8O_7{\cdot}x\text{Fe}{\cdot}y\text{NH}_3$. The AFC used in this study was obtained from Aldrich and is 98% pure. It contains 7.5% NH_3, 14.5%–16.0% Fe metal, and 75% hydrated citric acid. Its molecular mass is 384.1.

The calcination product was obtained by heating at 500°C for 1 h in ambient conditions. Prior to analysis, the calcination product was kept dry over silica gel. The green hydrated form used in this study is highly soluble in water. The multi-walled carbon nanotubes (MWCNTs) were purchased from Jiang Young Trade Co. in China, with a carbon basis of 95%, length of 1–10 μm, 3–5 walls, a density of 35 g/cm^3, and a loose agglomerate size of 1–3 mm. Sulfuric acid (98%), nitric acid (69%), and HCl (36.5%) were obtained from BDH Chemicals Ltd. in Poole, England. The sulfonated azo-based dye Direct red 81 (DR81), shown in Fig. 1, is poorly biodegradable due to its complex structure.

The nano-adsorbents were characterized using X-ray powder patterns obtained by a JSX-60 PA JEOL Diffractometer (Japan) with CuKα radiation (λ = 1.5416Å) and a Ni-filter. Scans in the range $4° \le 2\theta \le 60°$ with d-spacing and relative intensities (I/I_o) were compared to JCPDS standard diffraction patterns. The samples were mounted separately on aluminum stubs, evacuated to 10^{-3} Torr, and precoated with a uniform Au/Pd film (20 min total; 5 min for each of the four sides) in a sputter coater to minimize electron beam charging. The applied sputter voltage was 1.2–1.6 kV with a JOEL 35CF (Japan) SEM operating at 20 keV to obtain electron images. FTIR spectroscopy was performed using a Shimadzu infrared spectrophotometer (Japan) with a resolution of 4 cm^{-1}, measuring 4,000–400 cm^{-1} of lightly loaded (<1%) thin discs of spectroscopically pure and dry KBr-supported test materials. Thermal analyses (TGA and DTA) of the dried test samples were carried out using a Shimadzu Thermal Analyzer; model TGA-60H (Japan) with a heating rate of 10°C/min and a flow of air atmosphere 20 mL/min. Transmission electron microscopy (TEM) analyses were performed on a model CM200 (Philips) with an operating voltage (20–200 kV) providing a resolution of 2.4 Å. The lowering of DR81 absorbance was followed by an Agilent Technology, Cary 60 UV-Vis spectrophotometer among 200–800 nm with a maximum absorbance at λ = 508 nm. For simplicity, the acronyms of sample names are as follows: Fe_2O_3/CNT is a dried composite of 3 wt.% Fe_2O_3 on MWCNT, while 10Fe_2O_3/CNT is 10 wt.% Fe_2O_3 on MWCNT calcined at 420°C for 1 h in a static air atmosphere.

2.2. Functionalization of MWCNTs carbon nanotubes

The activation or functionalization process is conducted through oxidation methods [17,18], which can introduce

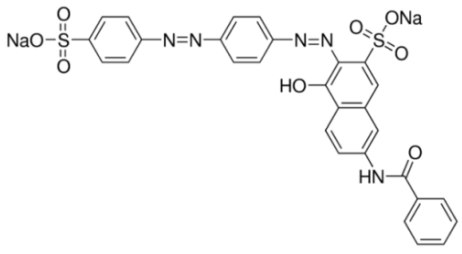

Fig. 1. Schematic of the Direct red 81 dye.

several functional groups on the carbon nanotube surface, including hydroxyl, carboxylic, ketonic, and oxygenated functional groups. Alcoholic and carboxylic functional groups on the surface facilitate the binding of nanoparticles to the nanotube surface. Therefore, in this study, MWCNTs were oxidized using a mixture of sulfuric and nitric acid (3:1 v:v). Oxidation using this mixture is preferred over other methods as it is expected to graft carboxylic and alcoholic functional groups onto the surface of the MWCNTs [19].

The oxidation process: 2 g of raw MWCNTs were mixed with 100 mL of a 3:1 (v:v) mixture of concentrated sulfuric acid (5.0 M) and concentrated nitric acid (5.0 M) in a round bottom flask. The reagents were sonicated for 15 min and then refluxed at 110°C for 3 h. The expected result of the oxidation process is the decoration of the MWCNTs surface with oxygen-containing groups. The separated solid material was soaked multiple times with deionized H_2O and dried under vacuum.

2.3. Synthesis of MWCNTs carbon nanotubes loaded Fe_2O_3

The synthesis of MWCNTs/MO requires that the nanotubes' surfaces have mainly alcoholic and carboxylic functional groups, which facilitate the binding process between Fe_2O_3 nanoparticles and nanotubes. CNTs loaded with Fe_2O_3 were prepared by dissolving calculated amounts of ammonium ferric citrate hydrate corresponding to loading levels of 3% (0.26 g of AFC) and 10% (0.868 g of AFC) weight percentages of Fe_2O_3 on CNTs as support in an appropriate volume of distilled water. The CNTs powder (2 g) was slowly sprayed for 15 min into the appropriate solution (300 mL) in parallel with continuous stirring. After the addition of CNTs was complete, the contents of the beaker were stirred for 1 h. The suspension of the CNT and AFC solution was left overnight in contact with the mother liquor at 110°C for drying purposes. Calcination of the dried products was conducted in a muffle furnace at a temperature of 420°C for 1 h in a static air atmosphere.

The synthesis strategy (Fig. 2) depends on the thermal analysis study of the parent materials. The thermal analysis chart of both MWCNTs indicates the stability of the compounds within the temperature range up to 420°C, which may guarantee the avoidance of damage or decomposition of carbon nanotubes at elevated temperatures.

2.4. Adsorption experiment

Adsorption studies of Direct red 81 (DR81) dye on MWCNT/Fe_2O_3 were carried out by varying different physiochemical conditions to explore the propensity of the adsorption technique. The kinetics of the adsorption studies were carried out by using a fixed adsorbent dose of 0.003 g and altering the initial concentration of DR81 to 14.7 mg/g in a 100 mL conical flask at a temperature ranging from 303 to 318 K. Each flask contained 0.003 g of various prepared samples, and 18 mL of water was added in a water shaker thermostat at a speed of 120 rpm for 1 h. Following each experimental run, 2 mL of a certain concentration of the dye solution was added, and then the sample solution was agitated intermittently between 2 to 200 min at a rate of 120 rpm. At certain intervals, the samples were filtered

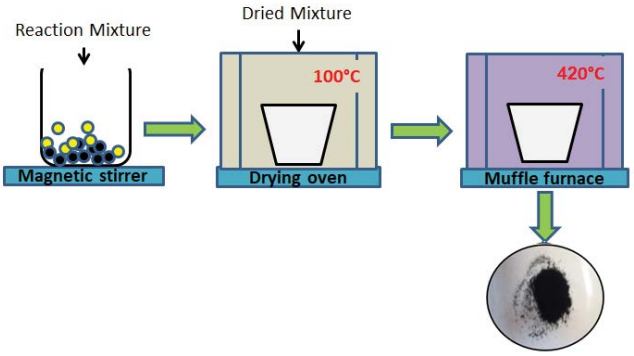

Fig. 2. Schematic presentation of the preparation process.

using a 0.45 μm Millipore filter, and the concentration of residual DR81 was recorded spectrophotometrically at a wavelength of 508 nm.

The average values of three repeated experimental runs were recorded. The amount of adsorbate dye per unit mass of the adsorbent (mg/g) was calculated using the following equation for time *t*:

$$q_t = \frac{\left(C_0 - C_t\right)V}{m} \tag{1}$$

where q_t is the value of the adsorption capacity of DR81 per unit mass of ($3Fe_2O_3$/CNT) (mg/g), V is the volume of the solution in liters, and m is the weight in grams. C_o and C_t represent the initial and equilibrium concentrations of the DR81 solution expressed in mg/L for time t. The efficiency of removal, expressed as a percentage (%), was calculated using the following equation:

$$R(\%) = \frac{\left(C_0 - C_t\right)}{C_0} \times 100 \tag{2}$$

Multiple parameters, such as dye concentration, pH level, amount of absorbent, contact time, particle size, and temperature, were varied during the experiment.

3. Results and discussions

3.1. Characterization of Fe_2O_3/MWCNTs

3.1.1. Transmission electron microscopy

The TEM image of Fe_2O_3/CNT clearly shows the loading of Fe_2O_3 nanoparticles on the surface of the carbon nanotubes. The acidic treatment, as well as the iron oxide precursor complex, provides functional groups with charges. After calcination, the Fe_2O_3 oxide formed as the final decomposition product from AFC, assembles on the surface of the tubes with a diameter of less than 10–30 nm, as displayed in Fig. 3.

3.1.2. Scanning electron microscopy

The morphologies of the prepared (Fe_2O_3/CNT) were examined using SEM at different magnifications, as shown

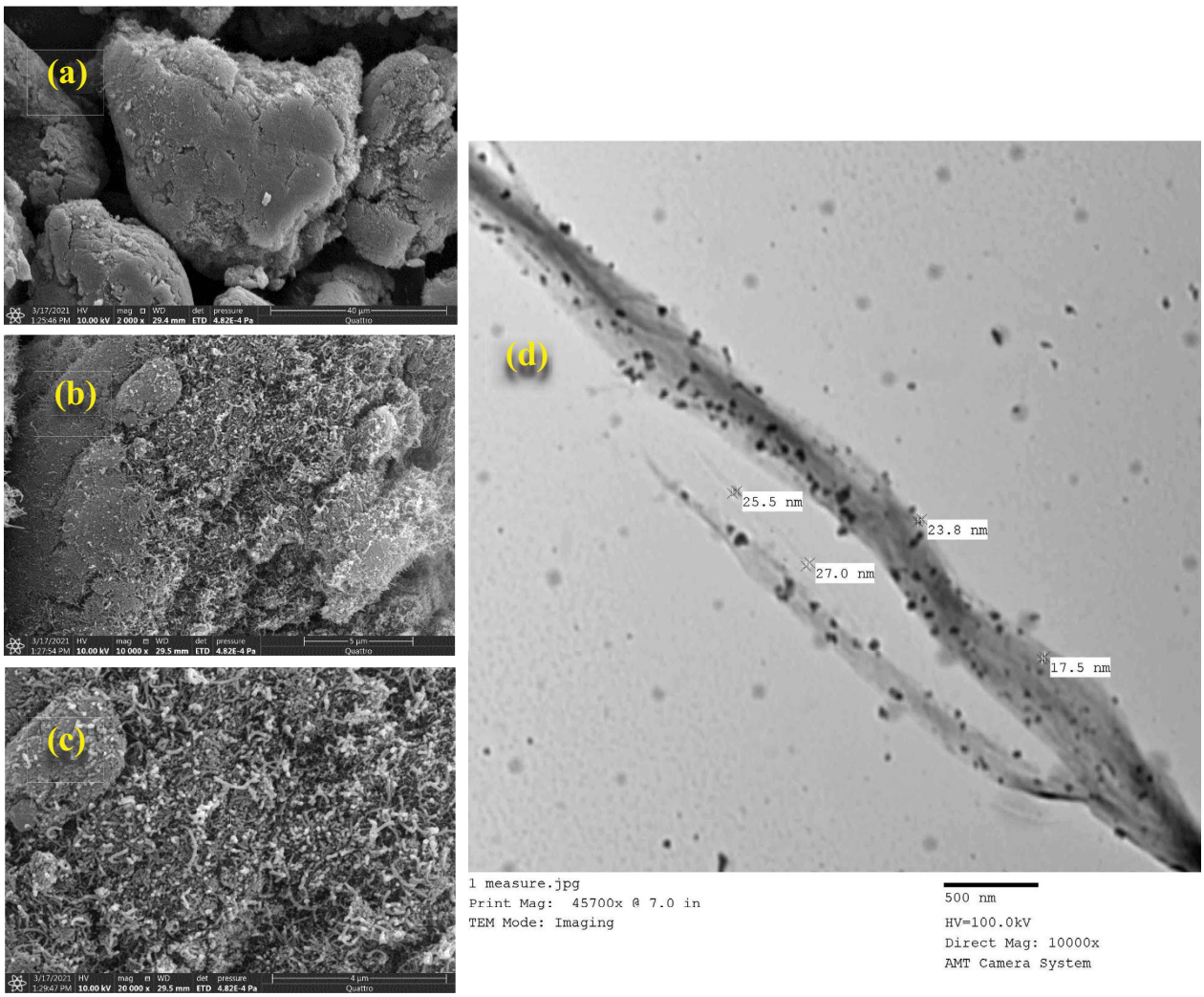

Fig. 3. Scanning electron micrographs (a–c) were recorded for Fe_2O_3/CNT at different magnifications and transmission electron microscopy image (d) of Fe_2O_3/CNT at 500 nm.

in Fig. 3. The acidified surface of the MWCNTs introduces polar hydroxyl and carboxyl groups, which are capable of interacting with Fe_2O_3 through hydrogen bonding. Fe_2O_3 nanoparticles successfully spread over the MWCNTs surface, forming a nanocomposite with a porous surface. Moreover, the SEM and TEM micrographs displayed in Fig. 3, respectively, demonstrate that there is no damaging impact due to the oxidation treatment using a mixture of nitric and sulfuric acids, as mentioned previously in the experimental section in detail.

3.1.3. Fourier-transform infrared spectroscopy

Fig. 4a–c display the FTIR spectra of three samples: acidified MWCNTs, Fe_2O_3/CNT, and $10Fe_2O_3$/CNT, respectively. The three spectra show similarity to a great extent (except for a few peaks), indicating that MWCNTs have been conserved during functionalization and support of the iron oxide Fe_2O_3 process. The spectra were conducted for a better comprehension of the composition and structure and to confirm the formation of iron oxide Fe_2O_3 from the ammonium iron citrate complex. Fig. 4a shows some changes in the intensity of bands representing the qualitative surface functional groups at 3,440; 2,987; 2,899; 2,318; 2,121; 1,683; 1,653; 1,570; 1,456–1,370; 1,066 and 542–503 cm^{-1}. The absorption band at 3,445 cm^{-1} is characteristic of –OH vibrations due to hydroxyl and carboxyl surface groups [20,21]. Furthermore, the bands at 2,899 and 2,987 cm^{-1} for –CH symmetric and asymmetric stretching of CH_2/CH_3 groups on the surface of MWCNTs are found because of some defects developed during the functionalization processes (Fig. 4a and b). The absorption bands at 1,697–1,653 cm^{-1} are most probably assigned to the stretching vibration of C–O and/or C=C groups attached to the surface of the nanotubes. The bands seen in the range of 800–500 cm^{-1} were assigned to Fe–O vibrational mode [22]. These peaks were clearly observed with the sample of higher loading of AFC ($10Fe_2O_3$/CNT). The above results thus indicate that the surface of the nanocomposites obtained properly contains groups of (–OH and COO–) [23–25]. When compared to the spectrum of functionalized MWCNTs, dissimilarities are observed in the intensities and structure of peaks.

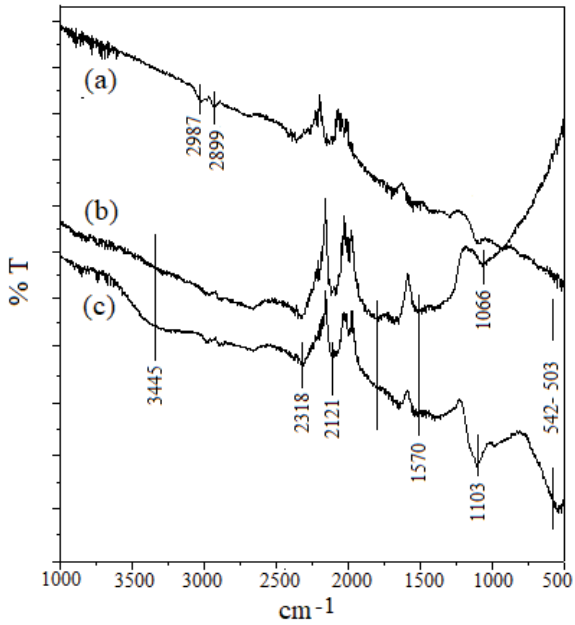

Fig. 4. Fourier-transform infrared spectra of acidified multi-walled carbon nanotubes (a), Fe_2O_3/CNT (b) and $10Fe_2O_3$/CNT (c), respectively.

3.1.4. Thermogravimetry

Thermogravimetry of the prepared composite was performed to test the stability of the active nanocomposite Fe_2O_3/CNT. 7 mg of the sample were heated in a Shimadzu Thermal Analyzer from ambient to 500°C in an air atmosphere with a heating rate of 10°C/min. The thermogram represented in Fig. 5 indicates that the nanocomposite is thermally stable up to the calcination temperature of 420°C. These results validate the success of the previously described preparation method. Evidently, MWCNTs are functionalized with many active groups, the presence of citrate moiety, as well as ammonia from AFC solutions, and the decomposition of such groups evolves many gaseous products. It is well-known that the evolution of gases may create porous and active surfaces. Moreover, the citrate group plays a major role in reducing the particle size of the generated oxide.

3.2. Adsorptive removal of synthetic dye

3.2.1. Change in intensity of spectra during adsorbent dye interaction

Pollutant dyes from the textile industry are a significant source of environmental contamination since they are often released into the environment in effluent. These effluents are toxic and mostly non-biodegradable. In this study, Direct red dye (DR81), an organic pollutant azo dye, was selected as the test degradable dye for the adsorption activity of the prepared composite MWCNTs/Fe_2O_3, abbreviated as Fe_2O_3/CNT. To assess the adsorption behavior of the prepared nanocomposite, 0.003 g of adsorbent was added to 14.77 mg/g of DR81 solution. A remarkable decrease in the absorption peak intensity of the dye was observed with progress in time. The decolorization rate of DR81 with the samples was

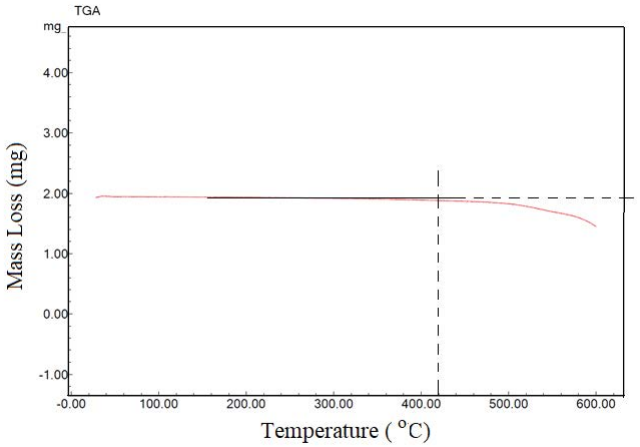

Fig. 5. Thermogravimetric analysis recorded for Fe_2O_3/CNT heat treated up to 600°C, at 20°C/min in air atmosphere (20 mL/min).

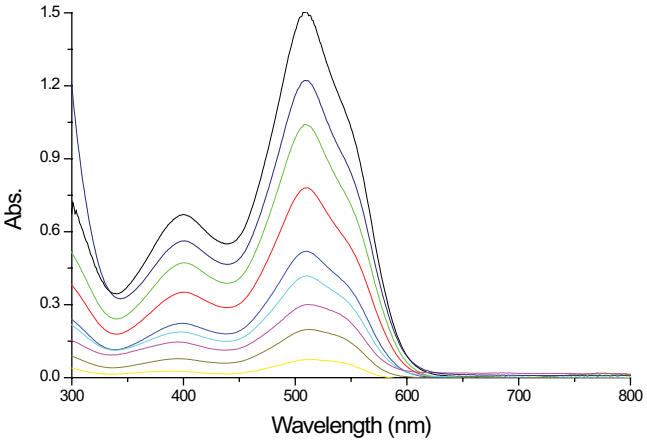

Fig. 6. The decolorization rate of Direct red 81 with the samples was followed spectrophotometrically at λ_{max} = 508 nm.

followed spectrophotometrically at λ_{max} = 508 nm, as shown in Fig. 6. The estimated contact time of the decolorization process is up to 2 h. Depending on the reaction conditions applied, the decrease in the absorbance of DR81 dye was approximately 80% of its original value. The molar extension coefficient of DR81 is ε = 47618.5 L/mol·cm. The concentration of the remaining dye in solution was calculated using Eq. (3), where V represents the volume of the solution in liters, m is the mass in grams of the nanocomposite, q_t is the adsorbed amount of the dye in mg/g at time t, and C_o and C_t are the initial and liquid phase concentration in mol/L at zero and at time t, respectively.

$$q_t = \frac{(C_0 - C_t)V}{m} \tag{3}$$

3.2.2. Effects of reaction parameters on DR81 dye

The following sections describe the effects of several factors on the reaction rate between DR81 and the

adsorbent nanocomposite, including the initial concentration of the dye, the amount of composite, the pH of the solution, and the temperature of the reaction.

3.2.3. Impacts of dye concentration and contact time

The removal of any dye is affected by the contact time at originally distinctive concentrations. In our experiment, the contact time intervals were arranged between 1 and 80 min. As the adsorbent material was exposed to DR81, a noticeable fast change in dye absorbance took place with time (Fig. 6). The decolorization process continued but at a slower rate as time passed. The process of decolorization appears to involve two steps. The first fast step may be attributed to the enormous number of active sites on the adsorbent surface. It took about 40 min to reach the pre-equilibrium requirements. As time passed, the number of adsorption sites available on the surface of the adsorbent decreased, resulting in a slowdown of the whole process.

The effect of the initial DR81 concentration (7.37, 11.08, 14.77, and 21.37 mg/L) on the adsorption efficiency of Fe_2O_3/CNT was evaluated on the basis that the initial concentration is the overall driving force. Fig. 7a clearly shows the decrease in adsorption efficiency of Fe_2O_3/CNT as the concentration raised from 7.37 to 21.37 mg/L, whereas the removal efficiency decreased from 77.34% to 54.8% against an increase in initial dye concentration. The experimental results verified that the initial concentration of dye affects the whole sorption efficiency of the adsorbent. As the initial concentration is high, the remaining dye concentration in the solution is consequently high, which results in lower sorption efficiency [26]. The results shown in Fig. 7a and b represent the removal of DR81 by sorption onto Fe_2O_3/CNT, explaining the above findings. However, due to the repulsive force between adsorbed and free molecules, the remaining vacant surface sites become less available for absorption over time. According to the reaction conditions applied, DR81 absorbance was decreased to almost 60%–90% of its initial value. In general, many parameters are associated with dye adsorption, such as surface charge, chemical composition, hydrophilic and hydrophobic properties, hydrogen bonding formation, and many other parameters [27,28].

3.2.4. Effect of adsorbent dosage

The adsorption efficiency of the nanocomposite adsorbents is greatly affected by the adsorbent dose. Various amounts of Fe_2O_3/CNT, from 2 to 7 mg, were added to an aqueous solution of DR81 (14.77 mg/L) at room temperature to equilibrium time. As observed from Fig. 8a and b, the efficiency of the removal process of DR81 increased from 58% to 90% with an increase in the amount of adsorbent. This may be attributed to the larger surface area occupying more adsorption sites.

3.2.5. Effect of temperature on the dye removal

The adsorption process is accompanied by enthalpy and entropy changes due to the effect of temperature during the decolorization process. The effect of solution temperature on the removal of DR81 dye with an initial concentration

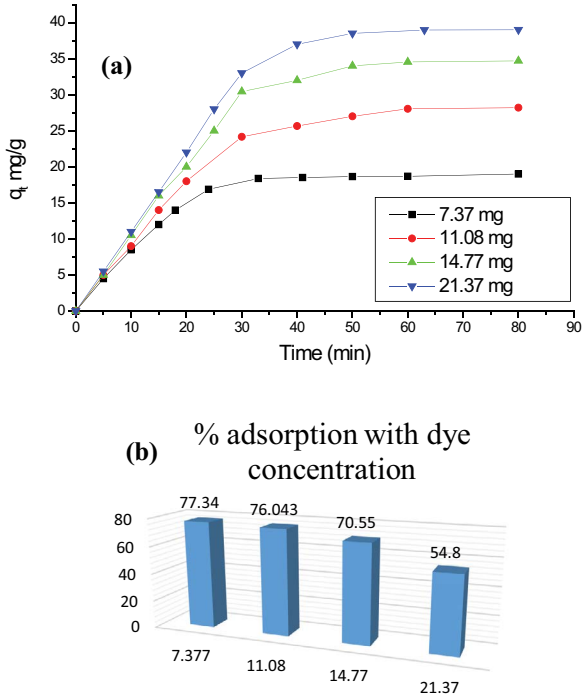

Fig. 7. Relation between contact time and adsorption efficiency of Fe_2O_3/CNT nanoparticles (5.0 mg) at 30°C (a), plot of the percentage adsorption of Direct red 81 for different dye concentration onto Fe_2O_3/CNT nanoparticles (5 mg) at 30°C (b).

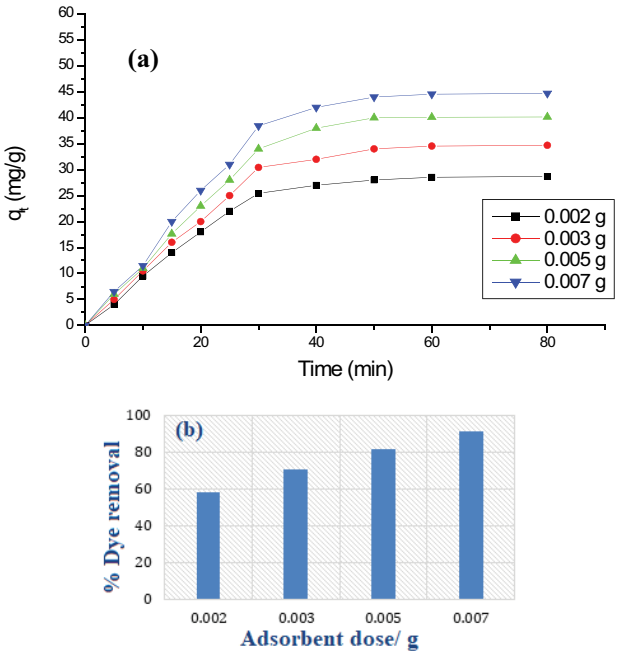

Fig. 8. Effect of composite dose on the equilibrium adsorbed amount of Direct red 81 dye onto Fe_2O_3/CNT nanoparticles at 30°C (a). The removed percentage of DR81 dye as a function of Fe_2O_3/CNT dose at 30°C (b).

(C_o = 14.77 mg/L) and 0.003 g of Fe_2O_3/CNT was studied in the temperature range of 30°C–45°C, while other parameters were kept constant. The results represented by (Fig. 9) indicate an increase in the adsorbed amount of DR81 on Fe_2O_3/CNT in the temperature range of 30°C–45°C. The adsorption process is sensitive to temperature change because temperature displays two major effects. The first effect increases the diffusion rate of the dye molecules across the boundaries of the solid adsorbent passing to its internal pores. The second effect is the effect on equilibrium capacity that may be displayed by adsorbents toward certain adsorbates [29–32]. The plot in Fig. 9a clearly shows an increase in removal efficiency from 60% to 82%.

3.2.6. Thermodynamic parameters

Thermodynamic parameters of the interaction between dye molecules DR81 and the adsorbent can be determined using thermodynamic equations. Predicting the mechanism of the adsorption process can be found via thermodynamic parameters, ΔG_{ads}, ΔH_{ads}, and ΔS_{ads}, which represent the free energy of the adsorption process, the enthalpy change, and the entropy change, respectively. These parameters can be calculated using the linear plot between $\ln(Q_e/C_e)$ and $1/t$, as given in Eqs. (4) and (5).

$$\ln\left(\frac{Q_e}{C_e}\right) = \frac{\Delta S_{ads}}{R} - \frac{\Delta H_{ads}}{RT} \tag{4}$$

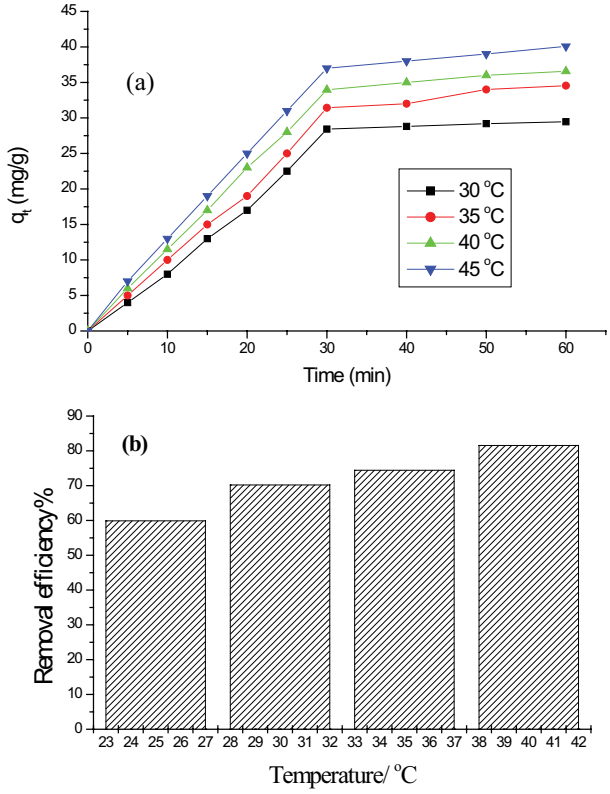

Fig. 9. Removed percentage of DR81 dye as a function of Fe_2O_3/CNT dose at 30°C (a), and plot of the percentage removal efficiency of Direct red 81 for different dye concentrations onto Fe_2O_3/CNT nanoparticles (0.003 g) (b).

$$\Delta G_{ads} = \Delta H_{ads} - T\Delta S_{ads} \tag{5}$$

The positive value for ΔH_{ads} (Table 1) indicates that the adsorption process is endothermic and is physisorption in nature, which is consistent with temperature effects. The negative values of the free energy change ΔG_{ads} reflect that the reaction proceeds without energy input (spontaneous process). Meanwhile, the positive value (Table 1) of the entropy changes ΔS_{ads} indicates the increased randomness at the solid-solution interface during DR81 adsorption on Fe_2O_3/CNT.

3.2.7. Effect of pH change parameter

The pH is a critical environmental factor that greatly affects the adsorbent surface and the absorbate in a solution. Varying pH values produce charges on the adsorbent surface and in the solution due to protonation or deprotonation of surface functional groups. Fig. 10a and b show the effect of pH change values on the adsorption process of DR81 using Fe_2O_3/CNT. The phosphate buffer solution with a concentration of 0.067 M was used to adjust the pH by adding a few drops of 0.1 M NaOH or HCl. The adsorption process was studied over pH ranges of 2 and 12. Fig. 10a shows that DR81 percentage removal displayed a marked increment at pH = 2 and then decreased with an increase in the value of pH until it reached pH = 9. Fig. 10b reveals the former explained change where the lowest dye adsorption was observed at pH = 9. The equilibrium uptake values were ~95% at pH = 2.5 and ~97% at pH = 12. It was found that the high adsorption at low pH values is attributed to the increase of positively charged H^+ ions on the surface of the adsorbent, which tends to sorb the dye molecules through electrostatic attraction [33]. The low sorption capacity as pH raised could be due to the decrease in the number of positive charge sites; that is, the surface charge density decreases due to the occupation of the adsorption sites by OH^- ions. This consequently prohibits the binding of anionic dye molecules onto the negatively charged adsorbent. Furthermore, at a pH higher than 9, the potency of adsorption enhanced again. The existence of excess OH^- ions in an alkali medium, rather than OH^- groups of the dye, can encourage interaction at higher pHs with the amine –NH function adsorbent groups, leading to higher adsorption [34,35]. The intermolecular hydrogen bonding between DR81 molecules is assumed to cause a multiple-layer creation in an aqueous solution, which illustrates the disparity among the adsorptive capability findings recorded at various pHs [17].

Table 1
Thermodynamic parameters of Direct red 81 adsorbed onto Fe_2O_3/CNT (0.003 g). C_o = 14.77 mg/L

Temp. (°C)	ΔH_{ads} (kJ/mol)	ΔG_{ads} (kJ/mol)	ΔS_{ads} (kJ/mol)
30	53.3	–23.3	235.05
35			
40			
45			

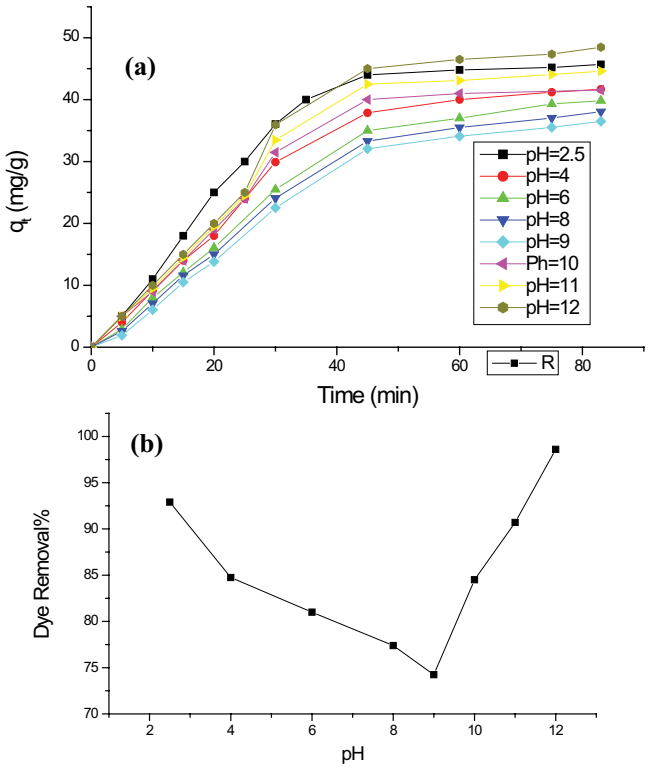

Fig. 10. Effect of different pH on the equilibrium adsorbed amount of Direct red 81 dye onto Fe_2O_3/CNT nanocomposite at 30°C, composite dose = 0.003 g. C_o = 14.77 mg/L (a), and removal efficiency of Direct red 81 (dye concentration = 14.77) from aqueous solution at different pH, amount of Fe_2O_3/CNT = 0.003 g, contact time = 30 min (b).

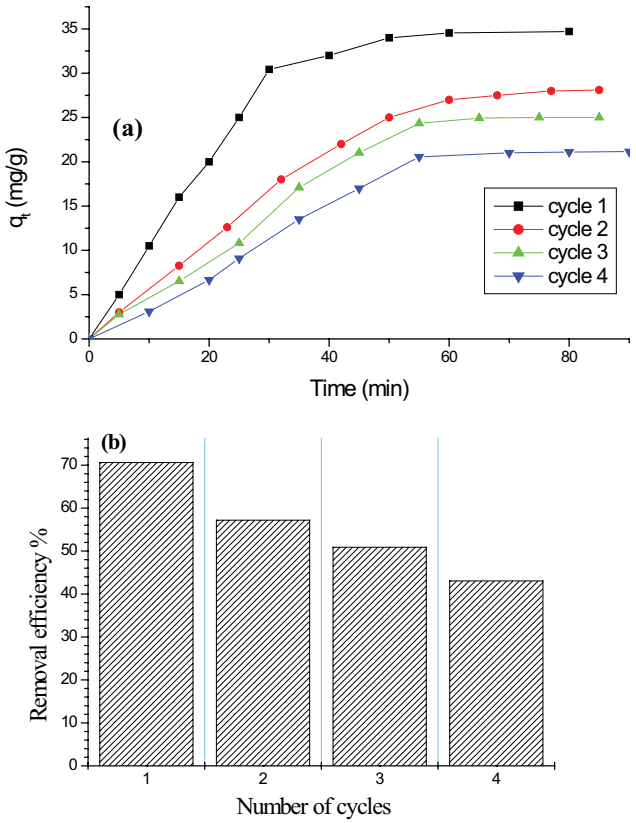

Fig. 11. Recycling studies for the adsorption of [DR81] $_o$ = 14.77 mg/L onto Fe_2O_3/CNT nanoparticles (0.003 g) at 30°C (a) and reusability of Fe_2O_3/CNT (b).

3.2.8. Reusability of carbon nanotubes loaded Fe_2O_3

Adsorbent reusability implies that the adsorbent can be regenerated and used over several cycles without a decline in performance. Economic feasibility is an important parameter for adsorption processes. The possibility of using Fe_2O_3/CNT adsorbent several times was tested. The used Fe_2O_3/CNT sample was prepared for reuse by washing with ethanol and distilled water and dried overnight to be used for a new cycle. The adsorption–desorption process was done four times, as shown in Fig. 11a and b. The sample displayed good stability, and its efficiency was still around 45% in the fourth cycle.

3.2.9. Adsorption isotherms

The Langmuir and Freundlich adsorption isotherm models were used to explain the adsorption of DR81 on carbon nanotubes loaded with iron oxide Fe_2O_3/CNT. The Langmuir isotherm provides the value of the R_L constant correlation factor, which decides the favorability of the adsorption process. R_L is given by Eq. (7), where the isotherm is favorable when ($0 < R_L < 1$), linear ($R_L = 1$), and unfavorable when ($R_L > 1$) [36]. The kinetic model assumes the existence of a homogeneously distributed finite number of active sites available as binding sites on the surface of Fe_2O_3/CNT.

$$\frac{C_e}{q_e} = \left(\frac{1}{K_L q_{\max}}\right) + \left(\frac{C_e}{q_{\max}}\right) \tag{6}$$

$$R_L = \frac{1}{\left(1 + K_L C_0\right)} \tag{7}$$

where q_e is the amount of dye adsorbed per specific amount of composite in mg/L, C_e is the concentration of the dye adsorbed in mg/L at equilibrium condition, K_L is the Langmuir equilibrium constant in L/g, and $q_{\max}$ is the Langmuir constant related to the theoretical maximum adsorption capacity in mg/g. The data in Table 2 indicate the favorable adsorption of DR81 on Fe_2O_3/CNT, with R_L = 0.1 at 30°C.

On the other hand, the linearized form of the Freundlich isotherm, Eq. (8) [37], is commonly used to depict the surface heterogeneity with multilayers of adsorbate and the exponential distribution of the active centers on surfaces.

$$\ln q_e = \ln K_F + \left(\frac{1}{n}\right) \ln C_e \tag{8}$$

where K_F and n are Freundlich constants representing the adsorption capacity in L/mg and intensity, respectively. q_e is the equilibrium constant when DR81 is adsorbed per gram of Fe_2O_3/CNT, and C_e is the equilibrium constant of DR81. Table 2 shows that the value of n is larger than one, suggesting the heterogeneity of the solid surface of Fe_2O_3/CNT, where a normal adsorption process was achieved.

The R^2 values (correlation coefficient) of the isotherms (Table 2) provide the suitability of the isotherm to describe

the absorption process. The fitting quality of the Langmuir and Freundlich isotherms was studied by comparing the value of R^2 of all the isotherms, and it was found that the Langmuir model has the noteworthy value of R^2. The R^2 values indicate that the Langmuir model fits better than the Freundlich model, suggesting that the adsorption of DR81 onto Fe_2O_3/CNT takes place via monolayer coverage on the surface without successive interaction between adsorbed species. The magnitude of n is larger than 1, proposing the heterogeneous surface of Fe_2O_3/MWCNTs corresponds to favorable adsorption. It was noticed that DR81 adsorption on the nanocomposite is quite consistent with the Langmuir model, not with the Freundlich model (Table 2).

3.3. Modeling of adsorption kinetics

The kinetics behavior was studied at 30°C using various initial concentrations of dye (Table 2). The kinetic models recommended to be utilized in studying the absorption mechanisms and determining the rate-controlling step of the reaction, as well as calculating the sorption parameters, including the equilibrium sorption capacity, rate constant, and initial sorption, from the experimental data. Eqs. (9) and (10) represent the pseudo-first-order model [38,39] and the pseudo-second-order models [40].

$$\log\left(q_e - q_t\right) = \log q_e \frac{k_1}{2.303} t \tag{9}$$

$$\left(\frac{t}{q_t}\right) = \left(\frac{1}{k_2 q_e}\right) + \left(\frac{t}{q_e}\right) \tag{10}$$

where k_1 and k_2 are the rate constants of the pseudo-first-order model in min^{-1}, and the k_2 is the rate constant of the second-order model in (g/mg·min). q_e and q_t are the amount of DR81 dye in mg/g absorbed at equilibrium on Fe_2O_3/CNT at equilibrium time and time (t), respectively.

Results in Table 2 show that the pseudo-second-order kinetic model fits the experimental data with an R^2 value of 0.998 and the calculated q_e values. The amount absorbed of dye on the composite surface shows good agreement with the experimental q_e values, and the correlation between q_o and q_{ads} measured at various concentrations of DR81 is presented in Fig. 12.

Table 2
Langmuir and Freundlich isotherms constants for the adsorption of Direct red 81 on Fe_2O_3/CNT nanocomposite

Adsorption isotherm	Parameters	Values of the parameters
Langmuir	q_m (mg/g)	40.05
	K_L (L/mg)	0.482
	R^2	0.994
Freundlich	K_F (L/mg)	70.81
	n	2.5
	R^2	0.985
		2.50

3.4. Adsorption mechanism

The absorption mechanism for dye removal includes three main consecutive processes. The first process is the transport of the dye molecules to the adsorbent surface via the boundary layer. The second is the transfer of dye molecules to the pores of particles through the mechanism of intraparticle diffusion, and then the third step is a surface reaction, adhering the dye particles to the surface active sites of the adsorbent.

The intraparticle diffusion model, represented by Eq. (11), is usually used to demonstrate the adsorption mechanism by a sorbent [41].

$$q_t = K_i t^{0.5} + C \tag{11}$$

where K_i is the rate constant of the diffusion kinetics represented by the intraparticle model measured in (mg/g·$min^{1/2}$), and C is the intercept. Fig. 13 describes the plot of K_{ads}, the fraction of the dye uptake at a time (t) vs. ($t^{0.5}$) to give K_i as a slope and C as the intercept. The first linear part of the

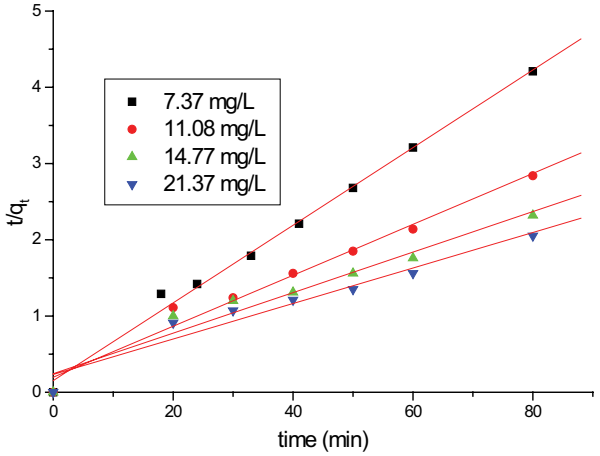

Fig. 12. Plot of q_t measured at different concentrations of Direct red 81 onto Fe_2O_3/CNT nanoparticles.

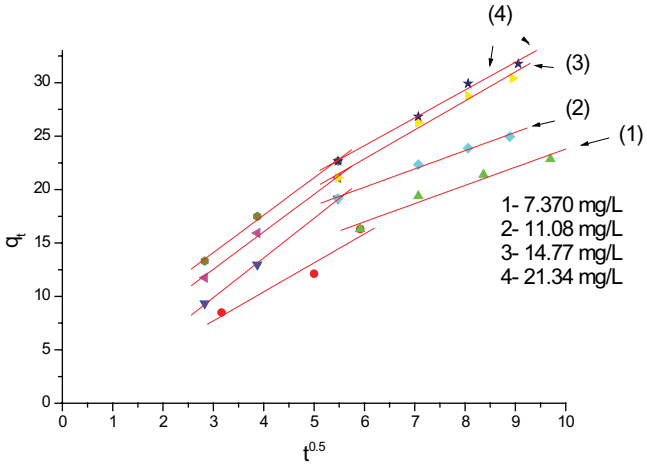

Fig. 13. Intraparticle diffusion model of adsorption of Direct red 81 on Fe_2O_3/CNT nanoparticle.

Table 3
Kinetic data with correlation coefficient (r) for the adsorption of Direct red 81 onto Fe_2O_3/CNT nanocomposites (0.025 g), at t = 30°C

Initial dye concentration (mg/L)	Pseudo-first-order model for adsorption			Pseudo-second-order model for adsorption				Intraparticle diffusion model for adsorption			
	q_e (mg/g)	k (min^{-1})	R^2	$q_{e,cal} \times 10^{-2}$ (mg/g)	$q_{e,cal}$ (mg/g)	$k_2 \times 10^{-2}$ (mg/g·min)	R^2	K_{p1} (mg/g·$min^{1/2}$)	r	K_{p2} (mg/g·$min^{1/2}$)	r
7.370	24.07	0.066	0.989	19.64	19.00	1.69	0.996	4.701	0.994	0.183	0.988
11.08	36.32	0.064	0.952	29.94	28.20	0.56	0.988	5.868	0.993	1.213	0.944
14.77	45.27	0.054	0.988	37.64	34.70	0.29	0.986	6.781	0.998	1.281	0.917
21.34	50.06	0.044	0.989	41.94	39.00	0.23	0.997	7.341	0.995	0.713	0.902

Table 4
Adsorption capacity of some previously studied adsorbents reported in the literature [44–47] toward the removal of Direct red 81 compared to the present study

Adsorbent	q_m (mg/g) DR81	References
Carbonaceous materials	33.67	[43,44]
Magnesium oxide-coated kaolinite	26.55	[45]
Iron filings	25.3	[46]
NaOH-modified rice husk	14.77	[47]
[Cu_2-L]@MWCNT	75.5	[17]
3Fe_2O_3/CNT (This study)	42.5	–

intraparticle diffusion plot (Fig. 13) shows the boundary layer influence on the absorption process described by k_1, indicating a fast rate of diffusion. The second linear part of the plot (Fig. 13) indicates the achievement of the diffusion of the molecules inside the pores of the composite and adsorbed by its interior surfaces. The second stage is slow, as indicated by k_2 (Table 3), because the diffusion resistivity increases due to the continuous uptake of the dye until the final equilibrium is reached [42]. The values of k_1 and k_2 were calculated from the slopes of the two linear portions of the plot (Fig. 13).

It is evident that the modified MWCNTs have a more specific surface area and better porous morphology that facilitate the adsorption of dye particles.

The adsorption efficiency percentages of the samples prepared for this study, including bare Fe_2O_3, 3Fe_2O_3/CNT, and 10Fe_2O_3/CNT, were calculated and found to be 24%, 43%, and 33%, respectively. The improved degradation performance is found with Fe_2O_3/CNT, which recommends that the smallest ratio of hematite addition provides a positive impact on the removal efficiency of the dye. A comparison of the maximum absorption capability for DR81 on different absorbents at room temperature is displayed in Table 4. It can be seen that the 3Fe_2O_3/CNT nanocomposite has good adsorption capacity compared to many previously utilized adsorbents.

4. Conclusion

Functionalized multi-walled carbon nanotubes (MWCNTs) were modified with 3% and 10% Fe_2O_3 nanoparticles and used as an efficient adsorbent for Direct red 81 dye. Fe_2O_3 was obtained from ammonium iron citrate as the precursor. The approach has the advantage of using a safe substance as well as saving costs by reducing the time and chemicals used. The synthesis strategy is simple and depends on the feasibility of ammonium citrate salt of iron. The adsorption isotherms of Direct red 81 (DR81) onto Fe_2O_3/multi-walled carbon nanotubes (Fe_2O_3/CNT) were evaluated under various adsorption conditions. The Langmuir and Freundlich adsorption isothermal models were used, and the equilibrium data showed that the Langmuir model was the one that fit linearly with the DR81 adsorption, while the highest adsorption capacity was 73.05 mg/g.

Furthermore, the kinetic studies of the adsorption process fit linearly with the pseudo-second-order model. In addition, the thermodynamic studies demonstrated an endothermic and spontaneous adsorption process with a negative value of free energy change, resulting in favorable adsorption. The positive values of ΔS and ΔH indicate increasing randomness at the liquid–solid interface.

Acknowledgments

The authors would like to thank the Deanship of Graduate Studies at Jouf University for funding and supporting this research through the Graduate Students Research support (GSR) program at Jouf University, Saudi Arabia. They would also like to express their appreciation to the central laboratory at Jouf University for providing analysis of the prepared samples.

Symbols

θ	—	Diffraction angle
d	—	Lattice spacing
T	—	Temperature in Kelvin
q_e	—	Equilibrium adsorption capacities
C_0, C_t	—	Primary and equilibrium concentrations of dye solutions
R	—	Removal efficiency, %
R^2	—	Correlation coefficients
ΔH	—	Standard enthalpy of reaction
ΔS	—	Standard entropy of a reaction
ΔG	—	Gibbs free energy change of the adsorption process
ΔE	—	Reaction activation energy
K	—	Reaction rate constant

K_i — Reaction rate constant of the diffusion kinetics
K_{ads} — Fraction of the dye uptake at a time, t

References

[1] S.E. Anderson, B. Jean Meade, Potential health effects associated with dermal exposure to occupational chemicals, Environ. Health Insights, 8 (2014) 51–62.
[2] P. Wycisk, H. Weiss, A. Kaschl, S. Heidrich, K. Sommerwerk, Groundwater pollution and remediation options for multi-source contaminated aquifers (Bitterfeld/Wolfen, Germany), Toxicol. Lett., 140–141 (2003) 343–351.
[3] T.A. Saleh, Protocols for synthesis of nanomaterials, polymers, and green materials as adsorbents for water treatment technologies, Environ. Technol. Innovation, 24 (2021) 101821, doi: 10.1016/j.eti.2021.101821.
[4] A. Mohammadi, P. Veisi, High adsorption performance of β-cyclodextrin-functionalized multi-walled carbon nanotubes for the removal of organic dyes from water and industrial wastewater, J. Environ. Chem. Eng., 6 (2018) 4634–4643.
[5] O. Duman, S. Tunç, T.G. Polat, B.K. Bozoğlan, Synthesis of magnetic oxidized multiwalled carbon nanotube-κ-carrageenan-Fe_3O_4 nanocomposite adsorbent and its application in cationic methylene blue dye adsorption, Carbohydr. Polym., 147 (2016) 79–88.
[6] L.Q. Ji, L.C. Zhou, X. Bai, Y.M. Shao, G.H. Zhao, Y.Z. Qu, C. Wang, Y.F. Li, Facile synthesis of multiwall carbon nanotubes/iron oxides for removal of tetrabromobisphenol A and Pb(II), J. Mater. Chem., 22 (2012) 15853–15862.
[7] S.A. Ntim, S. Mitra, Removal of trace arsenic to meet drinking water standards using iron oxide coated multiwall carbon nanotubes, J. Chem. Eng. Data, 56 (2011) 2077–2083.
[8] C.N. Li, J. Li, A.H. Liang, G.Q. Wen, Z.L. Jiang, Aptamer turn-on SERS/RRS/fluorescence tri-mode platform for ultra-trace urea determination using Fe/N-doped carbon dots, Front. Chem., 9 (2021) 613083, doi: 10.3389/fchem.2021.613083.
[9] W. Wu, Z.X. Geng, H.R. Bai, T. Liu, B.M. Zhang, Ammonium ferric citrate induced ferroptosis in non-small-cell lung carcinoma through the inhibition of GPX4-GSS/GSR-GGT axis activity, Int. J. Med. Sci., 18 (2021) 1899–1909.
[10] H.B. Wang, Z. Li, J.L. Niu, Y.F. Xu, M. Li, A.L. Lu, X. Wang, Z.K. Qian, Z. Huang, X. Jin, J.H. Wang, J. Zhong, B. Sun, G.X. Meng, Antiviral effects of ferric ammonium citrate, Cell Discovery, 4 (2018) 14, doi: 10.1038/s41421-018-0013-6.
[11] S.M. Park, Preparation of iron oxides using ammonium iron citrate precursor: thin films and nanoparticles, J. Solid State Chem., 9 (2009) 2456–2460.
[12] K.C. Verma, N. Goyal, M. Singh, M. Singh, R.K. Kotnala, Hematite α-Fe_2O_3 induced magnetic and electrical behavior of $NiFe_2O_4$ and $CoFe_2O_4$ ferrite nanoparticles, Results Phys., 13 (2019) 102212, doi: 10.1016/j.rinp.2019.102212.
[13] Y.X. Chen, H.C. Gu, Microwave assisted fast fabrication of Fe_3O_4-MWCNTs nanocomposites and their application as MRI contrast agents, Mater. Lett., 67 (2012) 49–51.
[14] J.H. Deng, X.H. Wen, Q.N. Wang, Solvothermal in situ synthesis of Fe_3O_4-multi-walled carbon nanotubes with enhanced heterogeneous Fenton-like activity, Mater. Res. Bull., 47 (2012) 3369–3376.
[15] D.H. Guan, Z. Gao, W.L. Yang, J. Wang, Y. Yuan, B. Wang, M.L. Zhang, L.H. Liu, Hydrothermal synthesis of carbon nanotube/cubic Fe_3O_4 nanocomposite for enhanced performance super capacitor electrode material, Mater. Sci. Eng., B, 178 (2013) 736–743.
[16] I.T. Kim, G.A. Nunnery, K. Jacob, J. Schwartz, X.T. Liu, R. Tannenbaum, Synthesis, characterization, and alignment of magnetic carbon nanotubes tethered with maghemite nanoparticles, J. Phys. Chem. C, 114 (2010) 6944–6951.
[17] R. El-Sharkawy, H.A. El-Ghamry, Multi-walled carbon nanotubes decorated with Cu(II) triazole Schiff base complex for adsorptive removal of synthetic dyes, J. Mol. Liq., 282 (2019) 515–526.
[18] S. N'goran Eroi, A.S. Ello, D. Diabaté, D.B. Ossonon, Heterogeneous WO_3/H_2O_2 system for degradation of Indigo Carmin dye from aqueous solution, S. Afr. J. Chem. Eng., 37 (2021) 53–60.
[19] H.-H. Cho, K. Wepasnick, B.A. Smith, F.K. Bangash, D. Howard Fairbrother, W.P. Ball, Sorption of aqueous Zn[II] and Cd[II] by multiwall carbon nanotubes: the relative roles of oxygen-containing functional groups and graphenic carbon, Langmuir, 26 (2010) 967–981.
[20] R. Sukor, N. Yusof, F.A. Azri, R. Hajian, Modification strategy of screen-printed carbon electrode with functionalized multi-walled carbon nanotube and chitosan matrix for biosensor development, Asian J. Chem., 29 (2017) 31–36.
[21] J.M. Tan, S. Bullo, S. Fakurazi, M.Z. Hussein, Preparation, characterisation and biological evaluation of biopolymer-coated multi-walled carbon nanotubes for sustained-delivery of silibinin, Sci. Rep., 10 (2020) 16941, doi: 10.1038/s41598-020-73963-8.
[22] S. Sahebian, S.M. Zebarjad, J. Vahdati Khaki, A. Lazzeri, The decoration of multi-walled carbon nanotubes with nickel oxide nanoparticles using chemical method, Int. Nano Lett., 6 (2016) 183–190.
[23] X.M. Sun, Y.D. Li, Colloidal carbon spheres and their core/shell structures with noble-metal nanoparticles, Angew. Chem. Int. Ed., 43 (2004) 597–601.
[24] S.X. Yang, L.Y. Wang, S. Yue, X.D. Guo, Y.F. Song, J. He, One-step solid-state synthesis of carbon nanotubes with surface functionality and their application in water treatment, RSC Adv., 3 (2013) 16990–16993.
[25] K. Krishnamoorthy, S.-J. Kim, Growth, characterization and electrochemical properties of hierarchical CuO nanostructures for supercapacitor applications, Mater. Res. Bull., 48 (2013) 3136–3139.
[26] M. Auta, B.H. Hameed, Modified mesoporous clay adsorbent for adsorption isotherm and kinetics of methylene blue, Chem. Eng. J., 219 (2012) 198–199.
[27] M. Auta, B.H. Hameed, Acid modified local clay beads as effective low-cost adsorbent for dynamic adsorption of methylene blue, J. Ind. Eng. Chem., 19 (2013) 1153–1161.
[28] B.K. Nandi, A. Goswami, M.K. Purkait, Adsorption characteristics of brilliant green dye on kaolin, J. Hazard. Mater., 161 (2009) 387–395.
[29] E. Rápó, S. Tonk, Factors affecting synthetic dye adsorption; desorption studies: a review of results from the last five years (2017–2021), Molecules, 26 (2021) 5419, doi: 10.3390/molecules26175419.
[30] R. Foroutan, S.J. Peighambardoust, S.H. Peighambardoust, M. Pateiro, J.M. Lorenzo, Adsorption of crystal violet dye using activated carbon of lemon wood and activated carbon/Fe_3O_4 magnetic nanocomposite from aqueous solutions: a kinetic, equilibrium and thermodynamic study, Molecules, 26 (2021) 2241, doi: 10.3390/molecules26082241.
[31] F. Güzel, H. Sayğılı, G.A. Sayğılı, F. Koyuncu, Elimination of anionic dye by using nanoporous carbon prepared from an industrial biowaste, J. Mol. Liq., 194 (2014) 130–140.
[32] Y.S. Ho, G. McKay, Sorption of dye from aqueous solution by peat, Chem. Eng. J., 70 (1998) 115–124.
[33] W. Konicki, D. Sibera, U. Narkiewicz, Adsorption of Acid Red 88 anionic dye from aqueous solution onto ZnO/$ZnMn_2O_4$ nanocomposite: equilibrium, kinetics, and thermodynamics, Pol. J. Environ. Stud., 26 (2017) 2585–2593.
[34] A.E. Yilmaz, R. Boncukcuoğlu, M. Kocakerim, I.H. Karakaş, Waste utilization: the removal of textile dye (Bomaplex Red CR-L) from aqueous solution on sludge waste from electrocoagulation as adsorbent, Desalination, 277 (2011) 156–163.
[35] T.A. Khan, S. Dahiya, E.A. Khan, Removal of Direct red 81 from aqueous solution by adsorption onto magnesium oxide-coated kaolinite: isotherm, dynamics and thermodynamic studies, Environ. Prog. Sustainable Energy, 36 (2017) 45–58.
[36] H. Kim, S.-O. Kang, S. Park, H.S. Park, Adsorption isotherms and kinetics of cationic and anionic dyes on three-dimensional reduced graphene oxide macrostructure, J. Ind. Eng. Chem., 21 (2015) 1191–1196.

[37] M.N. Carvallho, K.S. da Silva, D.C.S. Sales, E.M.P.L. Freire, M.A.M. Sobrinho, M.G. Ghislandi, Dye removal from textile industrial effluents by adsorption on exfoliated graphite nanoplatelets: kinetic and equilibrium studies, Water Sci. Technol., 73 (2016) 2189–2198.
[38] N.F. Al-Harby, E.F. Albahly, N.A. Mohamed, Kinetics, isotherm and thermodynamic studies for efficient adsorption of Congo red dye from aqueous solution onto novel cyanoguanidine-modified chitosan adsorbent, Polymers (Basel), 13 (2021) 4446, doi: 10.3390/polym13244446.
[39] X.B. Wu, K.N. Hui, K.S. Hui, S.K. Lee, W. Zhou, R. Chen, D.H. Hwang, Y.R. Cho, Y.G. Son, Adsorption of basic yellow 87 from aqueous solution onto two different mesoporous adsorbents, Chem. Eng. J., 180 (2012) 91–98.
[40] R. Aziam, M. Chiban, H. Eddaoudi, A. Soudani, M. Zerbet, F. Sinan, Kinetic modeling, equilibrium isotherm and thermodynamic studies on a batch adsorption of anionic dye onto eco-friendly dried *Carpobrotus edulis* plant, Eur. Phys. J. Spec. Top., 226 (2017) 977–992.
[41] Y.S. Ho, G. Mckay, Kinetic models for the sorption of dye from aqueous solution by wood, Process Saf. Environ. Prot., 76 (1998) 183–191.
[42] C. Namasivayam, M.V. Sureshkumar, Removal of chromium(VI) from water and wastewater using surfactant modified coconut coir pith as a biosorbent, Bioresour. Technol., 99 (2008) 2218–2225.
[43] A.N. Ebelegi, N. Ayawei, D. Wankasi, Interpretation of adsorption thermodynamics and kinetics, Open J. Phys. Chem., 10 (2020) 166–182.
[44] P. Shanthi, M. Karthik, K. Jothi Venkatachalam, S. Karthikeyan, Adsorption of acid blue 92 from aqueous solution using an activated carbon prepared from *Sterculia quadrifida* seed shell waste, J. Environ. Nanotechnol., 3 (2014) 96–104.
[45] T.A. Khan, S. Dahiya, E.A. Khan, Removal of Direct red 81 from aqueous solution by adsorption onto magnesium oxide-coated kaolinite: isotherm, dynamics and thermodynamic studies, Environ. Prog. Sustainable Energy, 36 (2017) 45–58.
[46] M. Dehghani, M. Nozari, A.F. Fard, M.A. Shiri, N. Shamsedini, Direct red 81 adsorption on iron filings from aqueous solutions; kinetic and isotherm studies, Environ. Technol., 40 (2019) 1705–1713.
[47] S.D. Ashrafi, H. Kamani, A.H. Mahvi, The Optimization of Direct red 81 and Methylene Blue Adsorption on NaOH-Modified Rice, Proceedings of the 14th International Conference on Environmental Science and Technology at Hens, Greece, 3–5, September, 2015.

Author Query

AQ1	Kindly provide the Manufacturer Location for the company “Aldrich”, “Agilent Technology, Cary 60 UV-Vis spectrophotometer”, “Philips”, “Millipore”.